Applied Bionics and Biomechanics
Vol. 5, No. 3, September 2008, 149–156

Taylor & Francis
Taylor & Francis Group

The SAHR setup–controlling hopping speed and height using a single actuator[1]

N. Cherouvim and E. Papadopoulos*

Department of Mechanical Engineering, National Technical University of Athens, Athens, Greece

(*Received 17 August 2008; final version received 20 October 2008*)

In this paper we present and experimentally validate a control method for regulating both the forward speed and the apex height of a one-legged hopping robot, using only a single actuator. The control method is based on a dynamic model of the hopping robot and makes use of the dynamic coupling of the vertical and forward motions of the robot. The control is applied first to a simulated model of the robot and shown to track a desired forward robot speed and a desired apex height. Then the SAHR (single actuator hopping robot) hardware is introduced and is used as an experimental platform with which to evaluate the performance of the control method. The control method is applied to the physical setup and is shown to lead to a stable hopping gait with a desired forward speed and apex height, despite the unmodelled disturbances met on the laboratory floor.

Keywords: legged; hopping; control; single actuator

Introduction

The purpose of achieving legged locomotion with robotic mechanisms has driven much research over recent years. Legged locomotion is a fascinating field of biomimetic robotics. Research has been conducted on a number of fronts, ranging from innovative robot designs to advanced control algorithms. It is indisputable that robots are faced with a much greater challenge than nature in the quest for successful locomotion. Mammals in particular possess admirable processing power and sensory feedback, and also, very importantly, they have many powerful muscles and degrees of freedom (DoF) available to perform locomotion. To the contrary, in robotics a large number of powerful actuators and the corresponding DoF are prohibitive due to cost, design complexity, weight, as well as problems of power autonomy.

To combat the problem of actuator weight and design complexity, a number of robot designs use only one actuator per leg for their locomotion (see Figure 1a). These include both six-legged robots and four-legged robots (Saranli et al. 2001; Talebi et al. 2000). Additionally, there has been considerable work on passive and semi-passive walkers, such as those of McGeer and others, some of which require no actuation at all but rather make use of the gravitational potential on a downhill slope (McGeer 1990; Tedrake et al. 2004). One problem with using a single actuator per leg is that the control problem becomes more complex, and though it may be possible to produce a stable gait, it is difficult to control both the forward speed and the height of the gait. Often, speed control is achieved by experimentation with control parameters, which can be effective but does not provide insight to the locomotion dynamics. Further understanding of how a single actuator can be used for the control of both the speed and the apex height is required.

One-legged robots are often used for developing and understanding the principles of legged locomotion (Raibert 1986; Ahmadi and Buehler 1997; Dummer and Berkemeier 2000; Hyon et al. 2003; Cherouvim and Papadopoulos 2005). Some work has indeed been done on the control of a hopping robot with one actuator, although the speed was not controllable in this case, and also with two actuators or by using two arms as well as the leg, in which case the forward speed can be controlled (Ahmadi and Buehler 1997, 1999; Cherouvim and Papadopoulos 2005; He et al. 2008). To date, it has not been possible to control both the forward speed and the apex height of a hopping one-legged robot, using only one actuator.

In this work we present a control approach for controlling both the forward speed and the apex height of a hopping robot that has only one actuator. We use this to show how the principle of regulated energy transfer between DoF can be implemented in a one-legged robot. Stable control is achieved by making use of the dynamic coupling of the forward and vertical motions of the robot, via the touchdown angle of the robot leg. The control algorithm is derived analytically, based on the robot dynamics of the robot model. As such, it requires no trial and error estimation of control gains, and may be applied to robots with different physical parameters without difficulty. The control validity is verified in simulations, and also in the SAHR experimental setup of a hopping robot with a single actuator. The control is shown to perform well both in simulation and when

*Corresponding author. Email: egpapado@central.ntua.gr

ISSN: 1176-2322 print / 1754-2103 online

DOI: 10.1080/11762320802564218
http://www.informaworld.com

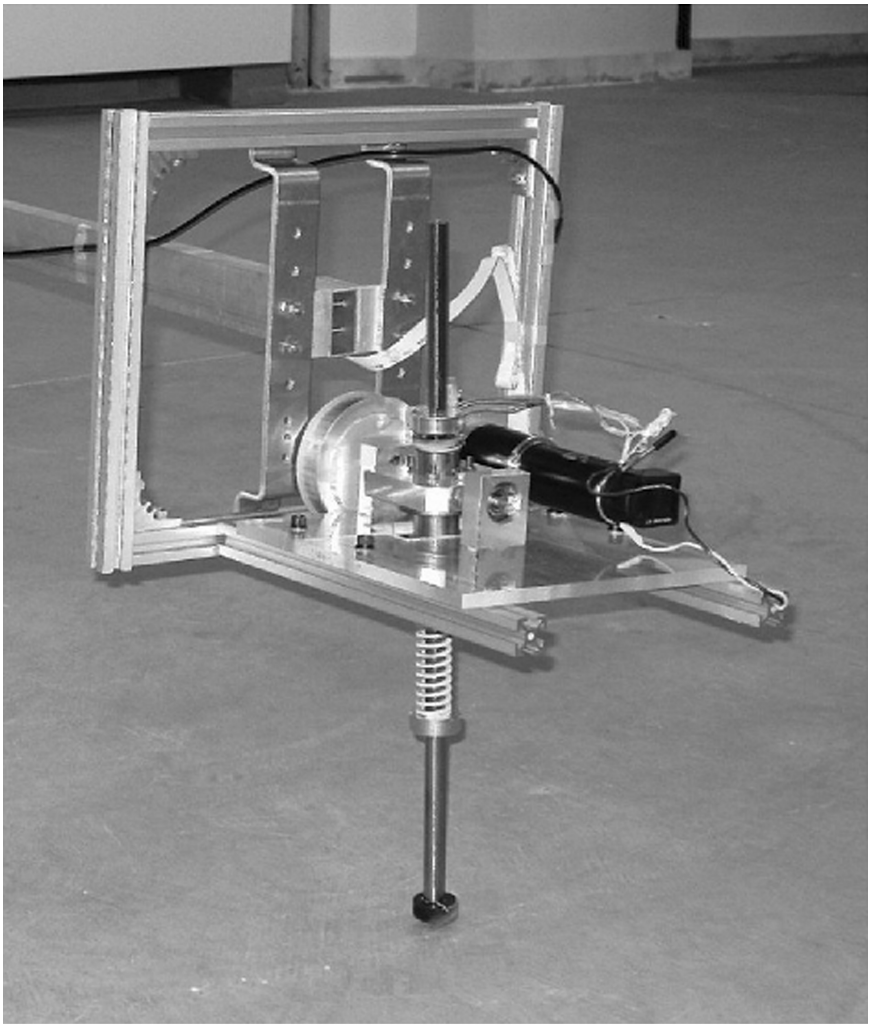

(a)

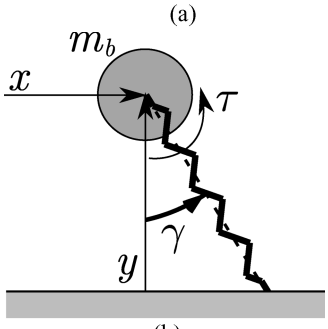

(b)

Figure 1. (a) The hopping robot, with a single actuator. (b) The two-dimensional robot model.

applied to the physical robot, despite disturbances in the laboratory environment.

Robot model and dynamics

In this work the one-legged robot we study is the SAHR (single actuated hopping robot). The complete setup is shown schematically in Figure 2, while the robot and its leg are shown in Figure 1a. Referring to Figure. 2, the robot motion is constrained by an arm that has a shoulder joint which permits vertical motion, while the whole body is free to rotate around a central pivot. This constrains the robot to perform a circular motion, and also the body pitching motion. Although the robot motion is circular, due to the small hopping

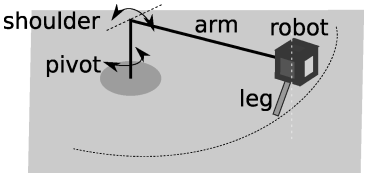

Figure 2. Schematic layout of the SAHR setup.

height and step lengths of the robot, it is common practice to consider that the hopping due to this type of constraint mechanism is planar (Raibert 1986). As a result, we study the dynamics of a planar model of the robot, and then test the results on the physical setup.

The planar model of the robot is shown in Figure 1b. The robot leg is considered to be massless, when compared to the much heavier body. The leg angle is actuated by a torque τ applied at the hip which is the only actuation, as in the SAHR setup. The leg also has an unactuated prismatic DoF, allowing it to compress or extend. This DoF is fitted with a linear passive spring of stiffness k and viscous friction is modelled in the prismatic DoF of the leg, with a viscous friction coefficient of b. The leg length is denoted by l and when the spring is uncompressed it has a rest length of L. Like the SAHR, the model does not involve body pitching. Finally, we also consider the effect of the inertia of the electric motor's rotor. This is significant due to the reduction of the planetary gearhead, as will be demonstrated later.

For the stance phase, when the leg is on the ground, we follow a Lagrangian approach for the derivation of the dynamics using the Cartesian coordinates x and y as generalised variables. The dynamics initially has a complex form, written using the Cartesian quantities x and y. However, observing that certain complex expressions of x and y, actually represent the leg length l and the leg angle γ, the stance phase dynamics can be greatly simplified:

$$\mathbf{M}\,[\ddot{x}\ \ddot{y}]^T = \mathbf{f}, \tag{1}$$

where the mass matrix $\mathbf{M}$ is a 2×2 matrix, with the following elements:

$$m_{11} = m_b + I_m\, n^2\, \frac{\cos^2\gamma}{l^2}$$

$$m_{12} = I_m\, n^2\, \frac{\cos\gamma \sin\gamma}{l^2}$$

$$m_{22} = m_b + I_m\, n^2\, \frac{\sin^2\gamma}{l^2}$$

and $m_{21} = m_{12}$, and the right-hand side of the dynamics is $\mathbf{f} = [f_1\ f_2]^T$ where

$$f_1 = -k\,(L-l)\sin\gamma + b\,\dot{l}\sin\gamma - \frac{\tau\cos\gamma}{l} - \frac{2\,I_m n^2 \cos\gamma\,\dot{l}\,\dot{\gamma}}{l^2}$$

$$f_2 = +k\,(L-l)\cos\gamma - b\,\dot{l}\,\cos\gamma - \frac{\tau\,\sin\gamma}{l} - \frac{2\,I_m n^2 \sin\gamma\,\dot{l}\,\dot{\gamma}}{l^2}.$$

As can be seen, the non-diagonal terms of the mass matrix are due to the inertia of the rotor motor, and also include the sine of the leg angle. As the leg angle is small throughout the motion, these terms are neglected and the mass matrix assumes a diagonal form. Further, in the right-hand side $\mathbf{f}$ of the dynamics in (1), the last term of both elements is due to the inertial properties of the motor rotor and is small compared to the strong spring forces, torque terms and viscous friction terms. As a result, the stance phase dynamics in (1) become

$$\left(m_b + \frac{I_m n^2}{l^2}\right)\ddot{x} + k\,(L-l)\sin\gamma - b\,\dot{l}\sin\gamma = -\frac{\tau\cos\gamma}{l} \tag{2}$$

$$m_b\,\ddot{y} - k\,(L-l)\cos\gamma + b\,\dot{l}\,\cos\gamma = -\frac{\tau\,\sin\gamma}{l} \tag{3}$$

where Equations (2) and (3) are associated with the robot's forward mode of motion and vertical mode of motion, respectively. During the flight phase, when the robot is not in contact with the ground, the dynamics of the robot are simple. The robot centre of mass (CoM) performs a ballistic trajectory. Then the equations of motion during flight are

$$\ddot{x} = 0, \tag{4}$$

$$\ddot{y} = -g. \tag{5}$$

Robot control

The control inputs to our system are the torque applied during stance at the robot hip and the angle with which the leg hits the ground. This last input is realised by servoing the leg to a desired touchdown position during the flight phase. We realise both control inputs using the single actuator by setting two discreet actuator tasks. During stance the actuator applies a commanded torque τ_{stance}, and during flight it servos the leg to a desired touchdown position.

To control the forward speed and the apex height of the hopping, we study the forward and vetical motion of the robot separately. We compute the control inputs for the next stance phase based on the state of the robot at the beginning of the flight phase, at the point where the leg is just lifting

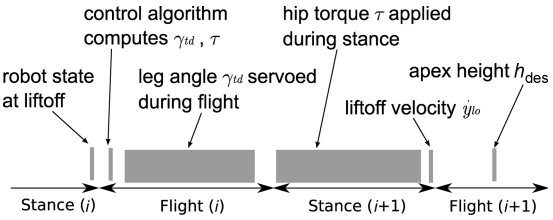

Figure 3. Schematic overview of the control events and method. The time line of the robot motion denotes the stance and flight phases.

off from the ground. For a schematic view of this see Figure 3.

First, we consider the control of the apex height. Achieving a desired apex height during flight is equivalent to achieving a desired vertical liftoff velocity $\dot{y}_{lo}$, at the end of the stance phase (see Figure 3). This is true since the flight dynamics are simple to integrate (see Equations (4) and (5)). To ensure a particular vertical velocity at liftoff, we start from the stance phase vertical dynamics given in Equation (3). Substituting the length l and the length rate of change $\dot{l}$ as a function of the coordinates x and y and using small angle approximations, the stance phase vertical dynamics from (3) yield

$$m_b\ \ddot{y} + b\ \dot{y} + k\ y = k\ L\ \cos\gamma. \tag{6}$$

In (6) the dynamics has the form of an oscillator driven by a term that involves the leg angle γ. However, it is not obvious how the oscillation can be controlled, as the leg angle is a continually changing quantity during stance. Due to the small angle simplifications, the actuator torque is not available as an input to the vertical dynamics. The evolution of the leg angle during stance can be predicted as (Raibert 1986)

$$\gamma = \gamma_{td} - \frac{\dot{x}}{L}\,t, \tag{7}$$

where γ_{td} is the leg touchdown angle and time t starts at leg touchdown. Substituting (7) in (6), the vertical dynamics takes the form

$$m_b\ \ddot{y} + b\ \dot{y} + k\ y = k\ L\ \cos\left(\gamma_{td} - \frac{\dot{x}\ t}{L}\right), \tag{8}$$

where time t starts from the beginning of the stance phase. We can now see that our second control input, the touchdown angle of the leg γ_{td}, appears as an input in the vertical dynamics. Using some minor approximations, it is possible to analytically integrate (8) twice. Then the leg touchdown angle γ_{td} can be computed such that a desired liftoff velocity $\dot{y}_{lo}$ is achieved, or equivalently such that a desired apex height h_{des} can be achieved

$$\gamma_{td} = f(\text{robot state at liftoff}, \dot{x}_{\text{des}}, h_{\text{des}}). \tag{9}$$

To control the forward speed, we start from the stance phase forward dynamics in (2), omitting the force term due to viscous friction in the leg which is small when compared to the large spring force. Also, for the terms associated with inertial forces or actuator torque, the compression of the leg is considered small. After small angle approximations, the stance phase forward dynamics is described by

$$\left(m_b + \frac{I_m n^2}{L^2}\right)\ddot{x} + k(L-l)\sin\gamma = -\frac{\tau}{L}. \tag{10}$$

Using (7) in (10) and integrating once, we acquire an expression that connects the forward speed of the robot at the beginning and the end of the $(i+1)$th stance phase (see Figure 3)

$$\dot{x}_{i+1,a} = -\int_0^{T_{st}} \frac{k}{m_{bx}}\left(\gamma_{td} - \frac{\dot{x}_{\text{des}}\ t}{L}\right)(L-l)\,dt - \int_0^{T_{st}} \frac{\tau}{m_{bx}\ L}dt + x_{i+1,b}, \tag{11}$$

where

$$m_{bx} = m_b + \frac{I_m n^2}{L^2} \tag{12}$$

and $\dot{x}_{i+1,b}$ and $\dot{x}_{i+1,a}$, are the forward velocity of the robot at the beginning and the end of the (i + 1)th stance phase, respectively. In (11) the touchdown angle γ_{td} is known from (9) and the evolution of the leg length can also be known from solving the vertical motion in (8). From (11) it is possible to analytically compute a constant torque τ_{stance} that must be applied throughout stance to achieve a desired forward speed $\dot{x}_{\text{des}}$ at the end of the stance phase. This provides the second input to the robot control

$$\tau_{\text{stance}} = f(\text{state at liftoff}, \dot{x}_{\text{des}}, h_{\text{des}}, \gamma_{td}) \tag{13}$$

Simulation results

First we test the control by simulating the robot model described earlier and shown in Figure 1b. The parameters of the simulated robot correspond to the actual SAHR experimental setup. The body mass is equal to $m_b = 3.8$ kg, the spring stiffness is $k = 4800$ N/m, the rest leg length is $L = 0.275$ m, and the coefficient of viscous friction in the leg is $b = 6$ Ns/m.

The control is applied to the robot model, and is made to follow a desired speed trajectory, while maintaining a constant desired apex height of 0.29 m. The initial conditions

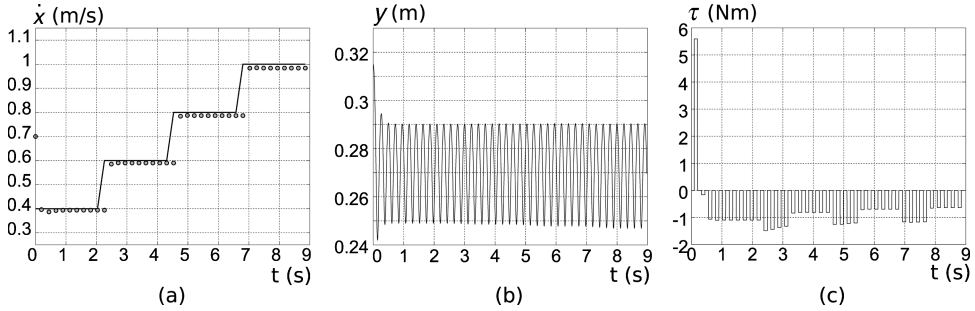

Figure 4. Simulation results of the control applied to the robot planar model. (a) The forward speed of the robot at each liftoff event with circles and the desired speed trajectory with a continuous line. (b) The vertical position of the robot body. (c) The torque applied by the hip actuator during each stance phase.

of the motion are not special. Results are shown in Figure 4. In Figure 4a, the forward speed of the robot is shown at each liftoff event with circles, while the desired speed trajectory is shown with a continuous line. It can be seen that the robot quickly tracks the desired speed trajectory. The apex height can be seen in Figure 4b to be kept constant at the desired value. Finally, Figure 4c shows the torque that was applied by the hip actuator during each stance phase. The small increases in the commanded torque are visible at the points in time where the desired forward speed is changed.

Experimental results

Experimetal setup

The experimental setup is shown in Figure 1a. The leg is constrained by the support arm to perform a cyclical motion around the main pivoting support. The processing power is a PC104 stack, running Linux, as well as a custom board of microcontrollers that implement the low-level interface with the sensors and the motor drive unit (see Figure 5a). The robot has two sensors which provide feedback for the control algorithm. The first feedback quantity is the angle of the leg with respect to the robot body, which is measured using a rotary optical encoder on the motor shaft. The second is the length of the robot leg, which is known indirectly from the leg compression. The leg compression is measured using the pseudo-knee mechanism shown in Figure 5b, which has a rotary optical encoder mounted at the knee joint. The leg compression is computed from the geometry of the knee mechanism. The feedback sensors used are easily transferable to the case of a fully autonomous robot.

The custom board of microcontrollers uses an I2C bus for data transmission. An Atmel AVR microcontroller serves as the I2C master, while PIC microcontrollers serve as I2C slaves. The I2C master is the only microcontroller to interface with the PC104 stack and this is accomplished using a custom interface that makes use of a GPIO (general purpose input output) card which is part of the PC104 stack. The I2C slaves are used for reading the two sensors and also for transmitting commands to the motor drive unit.

As mentioned, the main parameters of the SAHR hardware, m, k, L and b are those assumed for the robot model studied in the previous section. The only actuation of the SAHR is the electric motor used to actuate the leg angle DoF. The motor is a DC motor of Maxon motors, model RE35 (Maxon Motor AG 2008). The motor is coupled with a planetary gearhead, using a reduction ratio of 26:1. Also, a timing belt provides an additional reduction of 2:1, making the overall reduction from motor shaft to robot leg equal to 52:1. On the output shaft the system can produce a maximum of approximately 5.5 Nm of torque. The motor is driven by a Maxon ADS 50/5 motor drive used in torque control mode. Power for all components is provided from the mains. To compensate for the friction in the rotary DoF, a term of the form $b_{\text{rot}}\,\dot{\gamma}$ is added to the torque calculated by the control algorithm in (13). The commanded torque then takes the form

$$\tau_{\text{commanded}} = \tau + b_{\text{rot}}\,\dot{\gamma} \tag{14}$$

where τ is the torque computed by the control in (13). The coefficient b_{rot} is found experimentally to be 0.004 Nms/deg.

Results

The control is applied to the SAHR experimental setup. The control algorithm is run on the PC104 stack, and the aim is to maintain a desired forward speed $\dot{x}_{\text{des}}$ and a desired apex height h_{des}. In Figure 6 the response is shown, having set the desired forward speed to the value of 0.8 m/s and the desired apex height to 0.29 m.

In Figure 6a, the forward speed of the robot is shown to be around the desired value of 0.8 m/s, although some variations exist in the forward speed. The variations in speed are mainly due to the incline of laboratory floor where the robot was tested. As the robot is constrained to a

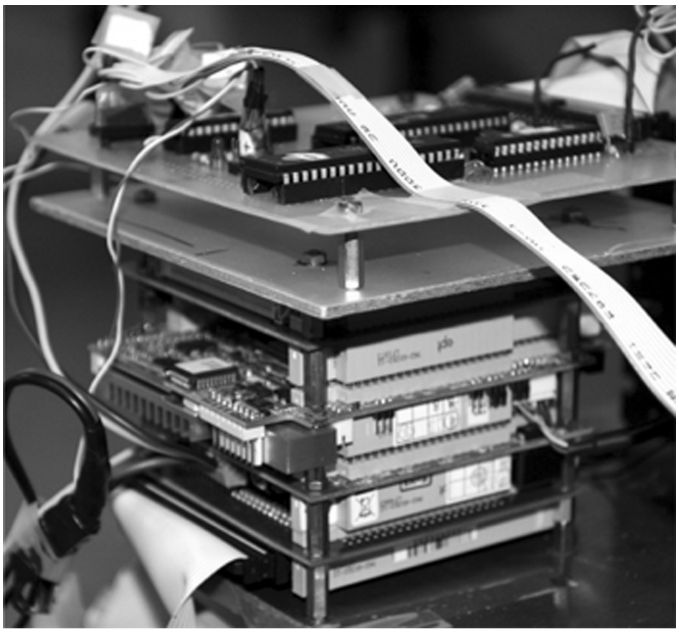

(a)

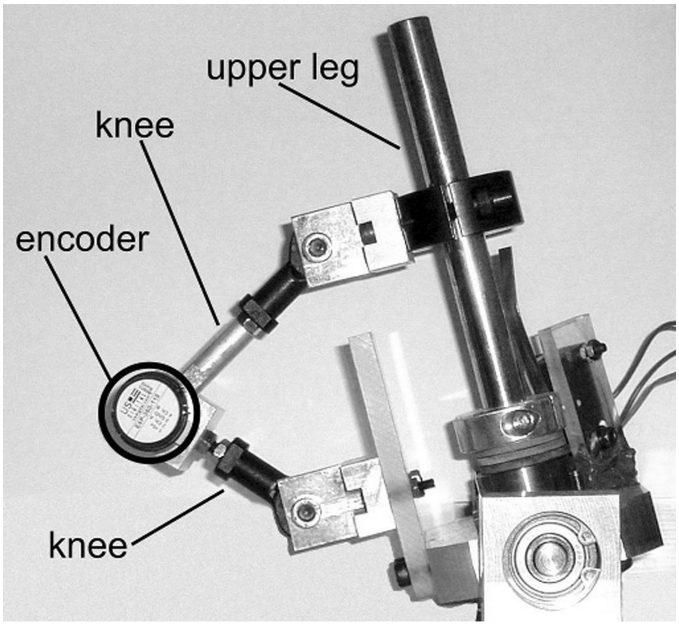

(b)

Figure 5. (a) The PC104 stack and the custom microcontroller board. (b) The pseudo-knee for measuring the leg length.

circular motion, the incline tends to accelerate or decelerate the robot, depending on its current position. Despite this perturbation, the control regulates the applied torque such that it continually returns the robot's forward speed to the desired value.

In Figure 6b, the apex height that the robot reaches during each flight phase appears to reach the desired value of 0.29 m, although periodic deviations from the desired value can be observed. These deviations are coupled to the changes in the forward speed of the robot. The control of the apex height assumes that the robot is running with its desired forward speed, and therefore deviations in the robots forward speed have a similar effect on the apex height achieved. It can be seen, however, that despite these deviations the control returns it close to the desired value. The maximum height that the robot can achieve is directly dependent on the torque that the actuator is able to provide.

Figures 6c and 6d show the inputs used to control the system, namely the torque exerted by the hip actuator during the stance phase and the leg touchdown angle which is set

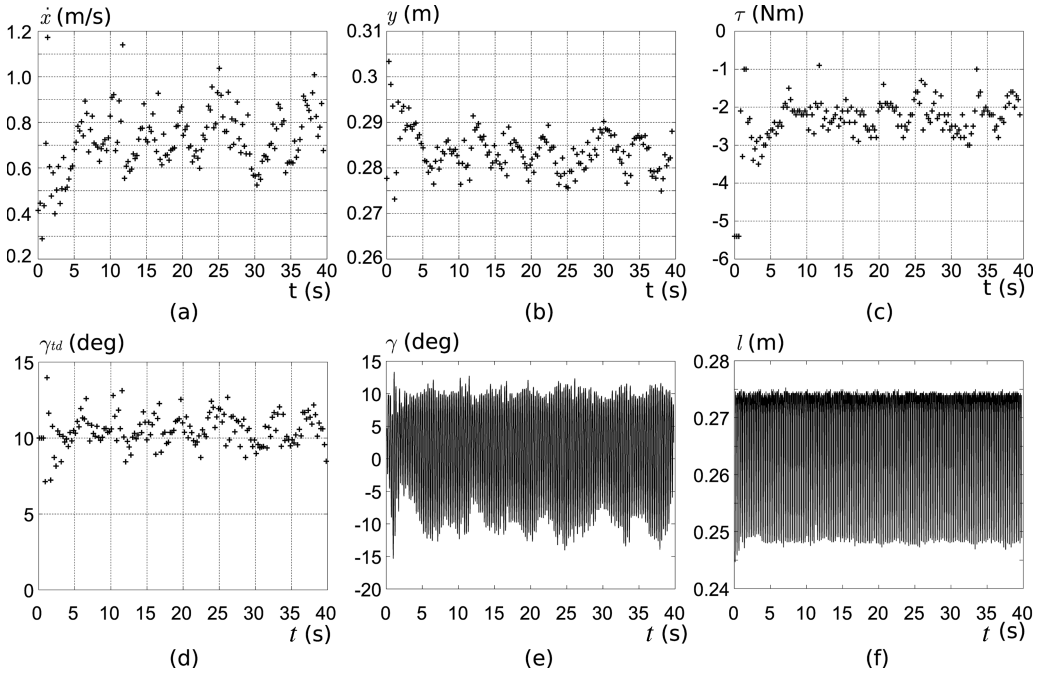

Figure 6. Response of SAHR setup to the control. a) The forward speed of the robot at each liftoff event. b) The vertical position of the robot body at the apex point of each flight phase. c) The torque applied by the hip actuator during each stance phase. d) The leg touchdown angle. e) The evolution of the leg angle γ in time. f) The evolution of the leg length l in time.

using the actuator during the flight phase. In Figure 6c the commanded torque surpasses 3.5 Nm only at the very beginning of the motion. Note that the commanded torque is given by (14). In Figure 6d the leg touchdown angle is shown to vary in a band of about 8–13 deg, after the initial 2 s of motion. A limit of 17 deg was placed on the value of the leg touchdown angle in the control software so as to avoid slipping, although it can be seen from Figure 6d that this limit was never reached.

Finally, in Figure 6e, the evolution of the leg angle γ is depicted, while in Figure 6f the length of the leg l is shown. From Figure 6e it can be seen that during the motion the leg performs an approximately symmetrical periodic motion about the zero angle. Additionally, Figure 6f shows the maximum compression of the spring element to steady during the entire motion and equal to about 0.025 m.

Conclusions

A control method was presented to allow the regulation of both the forward speed and the apex height of a one-legged robot, using only a single actuator located at the robot hip joint. To date, this has not been possible. The control approach is based on the dynamics of a planar robot model. The control was tested in simulation and it was shown that both the forward speed and the apex height of the body were tracked well. The control was also applied to the SAHR setup, and it was shown that it led to a stable gait, despite the unmodelled incline of the laboratory floor. Although there were small variations in the forward speed and the apex height of the robot, the control consistently kept the robot around the desired values.

Note

1. This work is co-funded by public funds (European Social Fund 80% and General Secretariat for Research and Technology 20%) and private funds (Zenon S.A), within measure 8.3 of Op.Pr.Comp., 3rd CSP - PENED 2003.

References

Ahmadi M, Buehler M. 1997. Stable control of a simulated one-legged running robot with hip and leg compliance. IEEE Transactions on Robotics and Automation vol. 13, pp. 96–104.

Ahmadi M, Buehler M. 1999. The ARL monopod II running robot: control and energetics. Proceedings of 1999 IEEE International Conference on Robotics and Automation. pp. 1689–1694.

Cherouvim N, Papadopoulos E. 2005. Single actuator control analysis of a planar hopping robot. Proceedings of Robotics: Science and Systems 2005, Cambridge, MA.

Dummer R, Berkemeier M. 2000. Low-energy control of a one-legged robot with 2 degrees of freedom. Proceedings of 2000 IEEE International Conference on Robotics and Automation, San Francisco, pp. 2815–2821.

Hyon SH, Emura T, Mita T. 2003. Dynamics-based control of a one-legged hopping robot. Proc Instn Mech Engrs. 217:83–98.

He GP, Tan XL, Zhang XH, Lu Z. 2008. Modeling, motion planning, and control of one-legged hopping robot actuated by two arms. Mechanism and Machine Theory 43. 33–49.

Maxon Motor AG. 2008. www.maxonmotor.com.

McGeer T. 1990. Passive dynamic walking. Int J Rob Res 9:62-82.

Raibert MH. 1986. *Legged robots that balance*, MIT Press, Cambridge, MA.

Saranli U, Buehler M, Koditschek DE. 2001. RHex: a simple and highly mobile hexapod robot. Int J Ro. Res 20:616–631.

Talebi S, Poulakakis I, Papadopoulos E, Buehler M. 2000. Quadruped robot running with a bounding gait. Proceedings of 7th International Symposium on Experimental Robotic (ISER^ž00), Honolulu, pp. 281–289.

Tedrake R, Zhang TW, Fong M, Seung HS. 2004. Actuating a simple 3D passive dynamic walker. Proceedings of the 2004 IEEE International Conference on Robotics and Automation, New Orleans, pp. 4656–4661.